CBN 95-14
Observations on proposed CESR Phase III Interaction Region Quads

G. Dugan

1. Basic requirements

The basic requirements are documented in the RFP[1]. The most fundamental requirement is that of the integrated field gradient. This comes, in principle, from the optical requirements necessary to match the insertion into the CESR lattice, and to achieve the required β^* at the IP (β^*_v = 7 mm, β^*_h = 1 m). The requirements are 30 T for the vertically focusing Q1, 24 T for the horizontally focusing Q2 and 3 T for the skew quad(SQ). Trims are required also, vertical and horizontal, of strength 0.03 T-m each. The quads are also to be rotated by 3^o, which introduces an additional skew quad field of 1.5 T from Q1 and 1.2 T from Q2.

The available slot length for these devices determines the required gradients. Assigned slot lengths[1] are 0.6 m for Q1 and Q2, 0.15 m for SQ and the trims. Assuming (optimistically) a magnetic length equal to the slot length, this sets the required field gradients at 50 T/m for Q1, 40 T/m for Q2, 20 T/m for SQ, and .2 T for the trims. It is clear that the trims, needing only 2 kG fields, could just as easily be resistive magnets, if slot length could be found for them outside the cryostat.

The final principal requirement for the quads is their clear aperture. They must have a warm bore, since beam-related radiation is sufficiently large to require extraction at room temperature. The minimum inner diameter of the warm bore is set by beam stay-clear requirements to be 110 mm in Q1 and 160 mm in SQ and Q2.

The inner diameter of the coil is not specified in the RFP. The radial clearance allowed for the warm bore is a significant design feature, since it drives the coil aperture. In the CERN LEP quad design[2], this radial clearance was 25 mm. They used 45 layers of aluminized kapton superinsulation, which was apparently sufficient. In the LEP200 design[12], the radial clearance was 20 mm. The RFP discusses water cooling of the bore tube. This may require more radial clearance. However, if we stick with 25 mm, it would put the inner coil diameter at 160 mm for Q1 and 210 mm for Q2.

Table 1
CESR Interaction Region superconducting magnet parameters

Magnet	Multi-polarity	Integrated field	Length	Gradient /Field	Bore id	Coil id
Q1	Quad	30 T	60 cm	50 T/m	110 mm	160 mm
Q2	Quad	24 T	60 cm	40 T/m	160 mm	210 mm
SQ	Skew quad	3 T	15 cm	20 T/m	160 mm	210 mm
H,V	Dipole	.03 T-m	15 cm	.2 T	160 mm	210 mm

Auxiliary requirements and/or operating parameters specified in the RFP include the following:

(a). Field quality: the higher multipole fields are required to be $<5x10^{-4}$ relative to the quadrupole field at a reference radius of 50 mm. This requirement ensures that the field errors do not compromise the dynamic aperture of the machine. Persistent current magnetization should be small (see section 5 below) so its time dependence should not be an issue.

(b). Alignment requirements: The alignment requirements are specified at 0.2 mm transverse, 0.5 mm longitudinal, and 0.2 mrad rotational. Presumably, the relative positioning of Q1, Q2 and SQ within the cryostat will not be adjustable after fabrication. Thus, in order to satisfy the requirements on the *relative* transverse and rotational alignment, the vendor must assure this sort of accuracy by mechanical design (liable to be costly), or he must measure the magnetic center and angle of each quad and place them within the cryostat with this accuracy. In addition, he must establish external fiducials on the cryostat, with the required precision, which can be used to reference the (cold) magnetic center and rotation of the assembly during installation.

With regard to the alignment requirements themselves, an error of 0.2 mm in Q1 placement, for example, produces a dipole field integral of about $6x10^{-3}$T-m (from Q1). This is well within the range of the correction dipoles, and so should be OK. However, in general the ultimate placement error of the quad magnetic center relative to the design reference orbit involves a contribution not only from the fiducial-field center error, but also from the error (which comes during installation) between the actual and design location for the fiducial in the tunnel-survey reference system. It is this total error which needs to be compared with the correction dipole strength. If the survey error was also 0.2 mm, then the overall error would be more like 0.34 mm, which is, however, still well within the correction dipole's range.

The longitudinal alignment requirement (0.5 mm) seems unnecessarily restrictive. Similarly, the stringent rotational alignment requirement appears very tight, in light of the strong skew quad available for correction.

The interfaces between the magnets and support systems are:

(i) Mechanical: Overall cryostat slot length 185 cm; outer diameter of the cryostat: 40 cm for Q1, 46 cm for SQ and Q2. The inner end of cryostat should be as close as possible to inner end of Q1. Mechanical interface details of the lead end of the cryostat, including power leads, cryo lines, instrumentation, etc. to be specified later. The cryostat itself must be non-magnetic, which rules out the (conventional) use of steel for the vacuum vessel. Other possibilities include stainless and aluminum. The LEP quads[2] used 304L SS for the vacuum vessel, and 304L and 314 L for the bore tubes; this material has a relative permeability of less than 1.025, which may be adequate.

(ii) Electrical: No requirements are given, since presumably the electrical system will be designed around the magnets. A preference for low current is suggested in the RFP. No requirements are set for voltage-to-ground during quench, although a low value for this quantity reduces insulation demands in the power bus and power supply .

(iii). Cryogenic: LHe at 4.6^{o}K, 1.4 bar available, as well as LN_2 at 2 bar. The refrigerator will presumably be able to satisfy the liquid mass flow and vapor (current lead) requirements. The expected cryostat heat leak is 20 W. There is no discussion of transfer line requirements, if any, between cryostat and refrigerator.

2. Similar magnets which have been built

Table 2 list several similar large-aperture SC quads and their major design features which have been built over the past 15 years. The examples which are closest in aperture to the CESR quads are the FNAL quads and the LEP quads. In both cases, the coils were wound with monolithic wire, rather than cable. The LEP quads used no iron and had a warm bore, making them the closest analog to the quads needed for CESR.

Table 2
Existing large-aperture superconducting quadrupoles

Descriptor	ISR IR quads	FNAL beam line quads	TRISTAN IR quads	RHIC IR quads	LEP IR quads	LEP 200 IR quads
Reference	9	8	4,5,6	7	2,3	12
Date built	1980	1983	1989	1993	1989	1994
Coil ID (mm)	230	150	140	130	180	160
Super-conductor	Mono-lithic MF wire	Mono-lithic MF wire	Cable	Cable	Mono-lithic MF wire	Mono-lithic MF wire
Bore	Warm	Cold	Warm?	Cold	Warm	Warm
Geometry	2 Blocks	1 block	4 shell	1 shell	2 Blocks	2 Blocks
Iron	Yes	Yes	No	Yes	No	No
Turns/pole	290	275		27	184	200
Length(m)	0.7	2.8	1.45	1.44	2	2
Operating current (kA)	1.6	0.9	3.4	5	1.6	1.9
Operating gradient(T/m)	43	50	70	48	36	60
Operating temp (º K)	4.3		4.5	4.6	4.3	4.3
Operating margin	12%	22%	21%	57%	50%	23%
Field quality (typical)	$<4\times10^{-3}$ @65mm	$<4\times10^{-3}$ @50 mm	$<5\times10^{-4}$ @40 mm	$<5\times10^{-4}$ @40 mm	$<3\times10^{-3}$ @50 mm	$<2\times10^{-3}$ @59 mm
Inductance (H)		1.12	.058		.23	.28
Cryostat OD (cm)	82	66	40		52	50
Cryostat heat leak @4K (w)	3-4		11		13	20
Cryostat quench pressure (bar)					3.5	
Peak temp. after quench		45ºK			200ºK	100-150ºK
Quench voltage					150 v.	200 v.

The quads made with wire ran at much lower currents than the cable quads. This is presumably because it was not possible to achieve a large number of turns with the cable. Lower currents are certainly much preferred from several points of view: for the magnet, for the cryogenic system, and for the electrical system. This would strongly favor wire as the conductor.

3. Model designs

It is possible to sketch a crude estimate of a 2-D design for the Q1 and Q2 quads using analytical formulae for fields in conductor-dominated magnets. The starting point is the vector potential for an infinitesimal line current dI (of infinite extent in the z-direction), located at coordinates (a, ϕ') in the x-y plane:

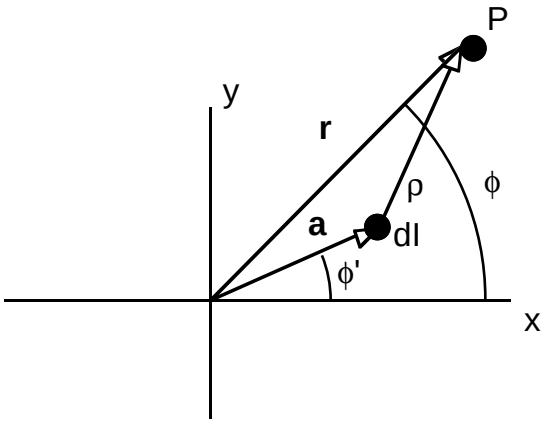

The vector potential at the field point P due to the line current dI is

$$d\vec{\mathbf{A}} = dA_z \hat{\mathbf{k}}$$

$$dA_z(r,\phi,a,\phi') = \frac{\mu_0 dI}{2\pi} \ln\frac{a}{\rho}$$

$$\vec{\rho} = \vec{\mathbf{r}} - \vec{\mathbf{a}}\,,\ \rho = \sqrt{r^2 + a^2 - 2arCos(\phi - \phi')}$$

The log can be expanded to separate variables:

$$\frac{dA_z(r,\phi,a,\phi')}{dI} = \frac{\mu_0}{2\pi}\sum_{n=1}^{\infty}\frac{1}{n}\left(\frac{r}{a}\right)^n Cos[n(\phi-\phi')] \quad \text{for} \quad r < a$$

$$= \frac{\mu_0}{2\pi}\left[\ln\frac{a}{r} + \sum_{n=1}^{\infty}\frac{1}{n}\left(\frac{a}{r}\right)^n Cos[n(\phi-\phi')]\right] \quad \text{for} \quad r > a$$

For a distribution of line current density in the x-y plane $J(a, \phi')$,

$$dI = J(a,\phi')adad\phi',$$

so the total vector potential from the current distribution is then

$$A_z(r,\phi) = \int_0^{\infty} ada \int_0^{2\pi} d\phi' J(a,\phi') \frac{dA_z(r,\phi,a,\phi')}{dI}$$

For a simple quadrupole single-shell geometry,

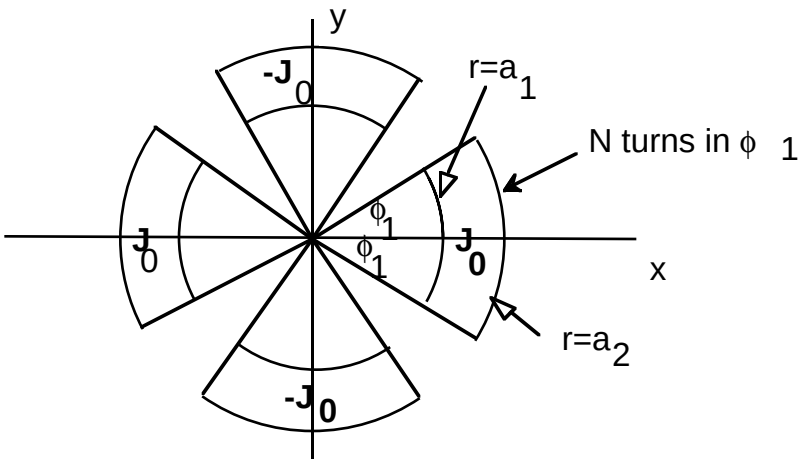

$$J(a,\phi') = \begin{cases} J_0 \text{ for } -\phi_1 \le \phi' \le \phi_1 \text{ and } -\phi_1 \le \phi' - \pi \le \phi \\ -J_0 \text{ for } -\phi_1 \le \phi' - \frac{\pi}{2} \le \phi_1 \text{ and } -\phi_1 \le \phi' - \frac{3\pi}{2} \le \phi \\ 0 \text{ for } r < a_1 \text{ and } r > a_2 \end{cases}$$

the vector potential becomes (see Appendix 1):

$$A_z^{coil}(r,\phi) = \frac{\mu_0 J_0}{2\pi} \sum_{m\ odd} \frac{1}{2m} R_m(r,a_1,a_2) \Phi_m(\phi,\phi_1)$$

in which the quantities $R_m(r,a_1,a_2)$ and $\Phi_m(\phi,\phi_1)$ are given in Appendix 1.

The field is given by

$$B_\phi(r,\phi) = -\frac{\partial A_z^{coil}}{\partial r}$$

$$= -\frac{\mu_0 J_0}{4\pi} \sum_{m\ odd} \frac{1}{m} \frac{dR_m(r,a_1,a_2)}{dr} \Phi_m(\phi,\phi_1)$$

$$B_r(r,\phi) = \frac{1}{r} \frac{\partial A_z^{coil}}{\partial \phi}$$

$$= \frac{\mu_0 J_0}{4\pi} \sum_{m\ odd} \frac{1}{m} \frac{R_m(r,a_1,a_2)}{r} \frac{d\Phi_m(\phi,\phi_1)}{d\phi}$$

For $r<a_1$, the quadrupole part of the field (m=1) is

$$B_\phi(r,\phi) = -r\frac{2\mu_0 J_0}{\pi}\ln\frac{a_2}{a_1}\mathrm{Sin}2\phi_1\mathrm{Cos}2\phi$$

$$B_r(r,\phi) = -r\frac{2\mu_0 J_0}{\pi}\ln\frac{a_2}{a_1}\mathrm{Sin}2\phi_1\mathrm{Sin}2\phi$$

which corresponds to a constant gradient

$$g = \frac{2\mu_0 J_0}{\pi}\ln\frac{a_2}{a_1}\mathrm{Sin}2\phi_1$$

If NI is the ampere turns/pole in the magnet, then the current density is given by

$$J_0 = \frac{2NI}{\phi_1\left(a_2^2 - a_1^2\right)}$$

and the gradient is related to NI by

$$g = \frac{4\mu_0 NI}{\pi\phi_1\left(a_2^2 - a_1^2\right)}\ln\frac{a_2}{a_1}\mathrm{Sin}2\phi_1$$

The effect of an iron shell at $r=R_e$, centered at r=0, can be included as described in appendix 2, for the case of iron with a homogeneous, isotropic permeability μ. For $r< R_e$, the presence of the iron results in an additional contribution to the vector potential,

$$A_z^{\mathrm{iron}}(r,\phi) = \frac{\mu_0 J_0}{2\pi}\frac{\mu-\mu_0}{\mu+\mu_0}\sum_{m\ \mathrm{odd}}\frac{1}{2m}R_m^{\mathrm{iron}}(r,a_1,a_2)\Phi_m(\phi,\phi_1)$$

in which $R_m^{\mathrm{iron}}(r,a_1,a_2)$ is defined in Appendix 2.

The total vector potential for points inside the cavity in the iron is then

$$A_z^{\mathrm{tot}}(r,\phi) = A_z^{\mathrm{coil}}(r,\phi) + A_z^{\mathrm{iron}}(r,\phi)$$

The gradient at $r<a_1$ is increased to

$$g = \frac{4\mu_0 NI}{\pi\phi_1\left(a_2^2 - a_1^2\right)}\ln\frac{a_2}{a_1}\mathrm{Sin}2\phi_1\left(1+\frac{\mu-\mu_0}{\mu+\mu_0}\frac{\left(a_2^4 - a_1^4\right)}{4R_e^4\ln\frac{a_2}{a_1}}\right)$$

The inductance per unit length of the magnet (L_l) can be calculated from these equations using the expression for the energy stored in the magnetic field. The details are in Appendix 3. The result is

$$L_1 = \frac{16\mu_0 N^2}{\pi\phi_1^2\left(a_2^2 - a_1^2\right)^2} \sum_{m\ odd} \frac{\mathrm{Sin}^2[2m\phi_1]}{m^3}\left(I_m^{coil}(r,a_1,a_2) + \frac{\mu-\mu_0}{\mu+\mu_0} I_m^{iron}(r,a_1,a_2)\right)$$

with $I_m^{coil}(r,a_1,a_2)$ and $I_m^{iron}(r,a_1,a_2)$ defined in appendix 3.

We apply the above relations to the magnets listed in Table 2 (except for the TRISTAN quads, for which the above model is a poor approximation to the 4-shell geometry), and to example designs for the CESR Q1 and Q2 quads: the results are given in table 3. The example designs for Q1 and Q2 use the same wire parameters as in the case of the LEP quads, with the coil id as listed in table 1, and the current required to give the desired gradients. For the other cases, the currents are as specified in table 2, and the gradients and fields are calculated from the above equations, assuming a uniform current density and a shell angle of 30º. The reason for this choice of shell angle is given in the next section.

In table 3, the outer coil radius is calculated from the number of turns and the wire area; the current density and gradient are calculated from equations above. The peak field occurs near $r=a_1$, and is calculated from the field equations given above. The field in the iron is the field at $r=R_e$, at the same azimuth as that of the peak field (about 30º). In general, in the table, the numbers in italics are calculated, the others are input.

Table 3
Model design parameters

Descriptor	**ISR quads**	**LEP quads**	**FNAL quads**	**RHIC quads**	**LEP200 quads**	**CESR Q1**	**CESR Q2**
Turns/pole	290	184	275	27	200	200	200
Wire area (mm^2)	6.4	6.4	4.2	11.9	5.8	6.4	6.4
a1 (mm)	115	90	75	65	80	80	105
a2(mm)	*143*	*112*	*100*	*74*	*104*	*106*	*126*
Re(mm)	200	-----	153	90	-----	------	175
I (amp)	1600	1600	905	5000	1900	1700	1700
g(T/m)	*43*	*38.2*	*48*	*50*	*60*	*52*	*40*
J(amp/mm2)	*250*	*250*	*215*	*420*	*327*	*265*	*265*
B-peak(T)	*5.9*	*4.2*	*4.1*	*3.95*	*5.7*	*4.9*	*5.05*
B-iron (T)	*2.56*	----	*1.45*	*2.4*	-----	----	*2.27*
length(m)	.7	2	2.8	1.44	2	.6	.6
L(H)	*.27*	*.26*	*.88*	*.006*	*.3*	*.09*	*.114*
W-stored (kJ)	*345*	*330*	*360*	*73*	*535*	*127*	*164*

Figures 1 and 2 show contour plots of the magnitude of the fields vs. r and ϕ in the model CESR Q1 and Q2 designs.

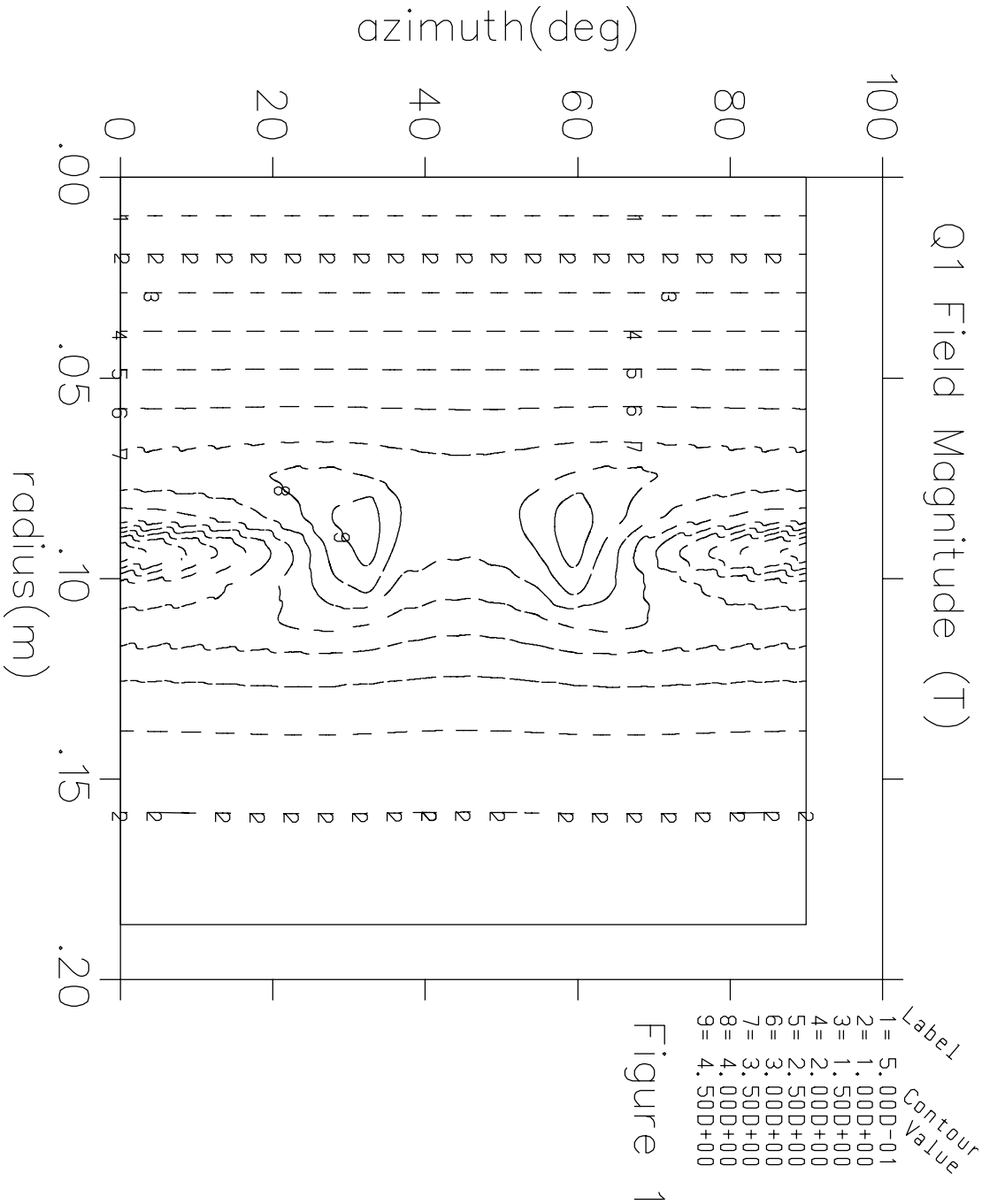
azimuth(deg)
0
20
40
60
80
100
.00
.05
.10
.15
.20
radius(m)
Q1 Field Magnitude (T)
Label
Contour Value
1= 5.000D-01
2= 1.000D+00
3= 1.500D+00
4= 2.000D+00
5= 2.500D+00
6= 3.000D+00
7= 3.500D+00
8= 4.000D+00
9= 4.500D+00

Figure 1

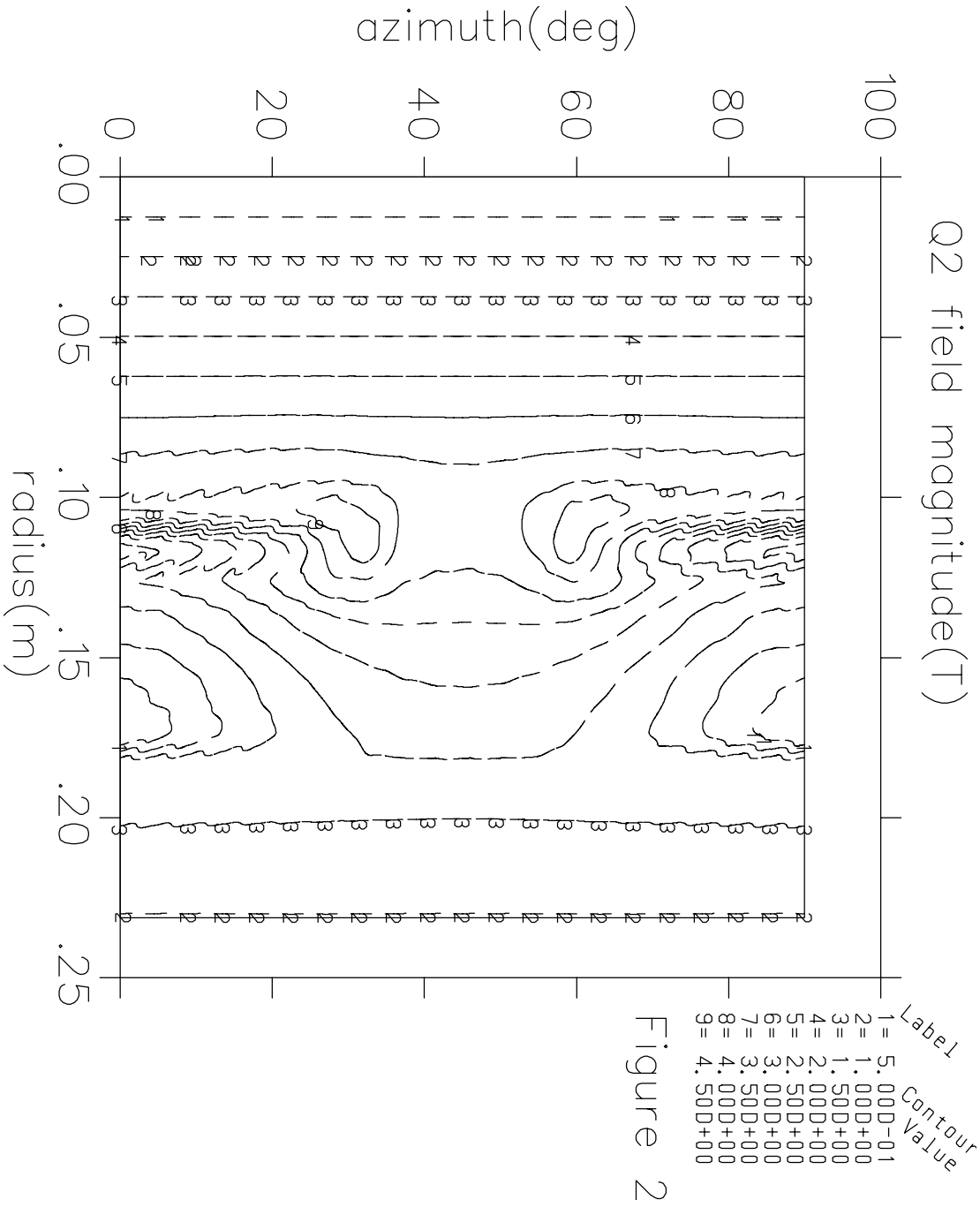
azimuth(deg)
0
20
40
60
80
100
.00
.05
.10
.15
.20
.25
radius(m)
Q2 field magnitude(T)
Label
Contour Value
1= 5.000D-01
2= 1.000D+00
3= 1.500D+00
4= 2.000D+00
5= 2.500D+00
6= 3.000D+00
7= 3.500D+00
8= 4.000D+00
9= 4.500D+00

Figure 2

4. Field quality in the body

The conventional expansion of the magnetic field in terms of normalized harmonic coefficients b_n and a_n, is

$$B_\phi(r,\phi) = B_0 \sum_{n=1} \left[\frac{r}{r_0}\right]^{n-1} \left(b_n \mathrm{Cos}(n\phi) + a_n \mathrm{Sin}(n\phi)\right)$$

$$B_r(r,\phi) = B_0 \sum_{n=1} \left[\frac{r}{r_0}\right]^{n-1} \left(b_n \mathrm{Sin}(n\phi) - a_n \mathrm{Cos}(n\phi)\right)$$

in which B_0 is the "reference field": for an n-pole magnet, the peak value of the n-pole field at the reference radius, r_0. In terms of the previously-developed expressions for the magnetic fields, we can get expressions for the field harmonics for $r<a_1$. The details are given in Appendix 4. The result is 0 for b_n, n odd, and $a_n=0$ for all n; for m=even, $b_{2m}=0$; for m odd,

$$b_{2m} = \frac{\left\{\left[\frac{r_0}{a_1}\right]^{2m-2} + \frac{\mu-\mu_0}{\mu+\mu_0}\left(\frac{a_1 r_0}{R_e^2}\right)^{2m}\left(\frac{a_1}{r_0}\right)^2\right\}}{m\left\{1+\frac{\mu-\mu_0}{\mu+\mu_0}\frac{a_1^4}{R_e^4}\right\}} \frac{\mathrm{Sin}\ 2m\phi_1}{\mathrm{Sin}\ 2\phi_1}$$

Choosing ϕ_1 such that $\phi_1 = \frac{\pi}{2m_0}$, for the smallest allowed harmonic m_0, will suppress that harmonic due to the $\mathrm{Sin}(2m\phi_1)$ term in b_{2m}. All harmonics which are integer multiples of m_0 are also suppressed. Thus, for m_0 =3 in the quadrupole case, choosing $\phi_1 = \frac{\pi}{6}$ suppresses m=3, 9, 15, etc. This leaves m=5 and m=7 as the lowest non-zero harmonics. Of course, this all assumes perfect quadrupole symmetry is maintained: otherwise odd-n b_n, even-m b_{2m}, and skew terms a_n will arise.

One simple measure of the sensitivity of the harmonics to symmetry violations is to let ϕ_1 deviate from 30 ^{o} and calculate the resulting b_6, and b_{18} terms. In table 4, we give, for the parameters for each quad listed in table 3, the calculated multipole coefficients b_{2m}, assuming the simple 30^o shell geometry (which of course, no real magnet has), and also the values of b_6 and b_{18} if an error of 0.5 mm is made in the arc length of the shell, causing it to deviate from 30^o. The calculated errors are smaller than those of an as-built magnet (shown in the last column), presumably due to minor design differences, manufacturing errors, and end effects, which can easily dominate the "theoretical" body field errors. Nevertheless, the calculation is useful in getting a feel for the expected error scale and tolerances required. The strong dependence on coil radius is evident in the small numbers for the CESR Q2 magnet.

The field quality achieved, for example, for b_6, for the LEP200 quads, was (on average over 8 magnets) about 14×10^{-4} @ 59 mm[12]. In the model used for table 4, this would correspond to an arc length error of about (14/21)*.5=.3 mm. If the CESR Q1 and

Q2 quads were built to the same level of mechanical tolerance, the resulting b_6 terms would be (14/21)*10=7x10^{-4} @ 50 mm for Q1 and (14/21)*3=2x10^{-4} @ 50 mm for Q2. Thus, the specified requirements of 5x10^{-4} @ 50 mm for Q1 and Q2 require tolerances roughly the same as that achieved for the LEP200 quads.

This argument, of course, assumes all the errors are in the body. Actually, end field errors may dominate, in which case the situation for the shorter CESR quads will be worse.

Table 4
Harmonics x10^4

Quadrupole	**r_0 (mm)**	**b_6 (δ=0.5 mm)**	**b_{10}**	**b_{14}**	**b_{18} (δ=0.5 mm)**	**b_n (typical)**
ISR quads	65	-5	-7	.3	-.001	<40
LEP quads	50	-6.7	-7	.3	-.001	<30
CESR Q1	50	-10.	-13.2	.85	-.006	
CESR Q2	50	-2.9	-2	.05	0.	
FNAL quads	50	-12	-20	1.5	-.015	<40
RHIC quads	40	-14.	-18	1.4	-.018	5
LEP200 quads	59	-21.	-57.	6.9	-.10	<20

5. Persistent current magnetization.

Long-lived eddy currents are induced within the superconducting filaments (called "persistent currents") as a superconducting coil is energized. These currents flow in such a way as to attempt to shield the interior of the superconducting filament from the applied field. The persistent currents flow at the maximum current density which the filament can support in the applied field at the operating temperature: this current density is called the critical current density. At applied fields above a few tenths of a Tesla, the persistent currents entirely fill the filament volume, flowing down one side of the filament and back the other side. This current pair constitutes a magnetic dipole. The overall net magnetization (magnetic moment per unit volume) from a single filament can be shown[10] to be

$$M_p = \frac{4}{3\pi} J_c(B) \varepsilon a$$

in which $J_c(B)$ is the critical current density, a is the radius of the filaments, and ε is the fraction of the wire which is superconductor. In general, as discussed below, $J_c(B)$ will decrease with B.

The fields generated by these persistent currents will contribute to the field errors discussed above. In general, the leading order field error due to the persistent currents will be the first allowed harmonic (after that of the main field): that would be b_6 (the duodecapole moment) in the case of a quadrupole. The general scale of the relative errors

generated by the persistent currents can be determined by calculating the ratio of the field associated with the persistent current magnetization ($\mu_0 M_p$) to a typical peak field:

$$\delta_{pc} = \frac{4\mu_0}{3\pi B} J_c(B) \varepsilon a$$

in which B is, for example, the peak field. The effect can be suppressed by reducing the filament radius a, although not without limit[10]. In Table 5, I calculate this quantity for the different quads. The filament sizes and superconductor fraction (in the form of Cu:Sc ratio) assumed are given in table 5: for FNAL, I just used the same as that for LEP quads. The dependence of the critical current density on B, and its value at a reference B and T, are taken as described in the next section.

Table 5
Persistent Current Magnetization

Quadrupole	**Filament radius (μm)**	**Cu:Sc ratio**	**$J_c(B_{peak})$ (A/mm^2)**	**B_{peak} (T)**	$\mu_0 M_p$ **(T)**	δ_{PC}**(x10^4)**
ISR quads	25	1.7	1038	5.9	.00513	8.7
LEP quads	18	1.7	1452	4.2	.00516	12.6
CESR Q1	18	1.7	1143	4.9	.00406	8.3
CESR Q2	18	1.7	1110	5.1	.00395	7.7
FNAL quads	18	1.8	1328	4.2	.00455	10.8
LEP 200 quads	20	1.7	1230	5.7	.00486	8.6

This simple calculation probably overestimates the magnitude of the effect. The scale is typically that of the geometric errors. This problem is typically much worse in magnets which must have a large dynamic range in field, because at low fields $J_c(B)$ increases, making δ_{PC} large: in this case the geometric multipoles are much smaller than the persistent current multipoles. However, in the CESR quads, which are used only at "full field", the problem should not be significant. It should be noted that the persistent currents die away on time scales of hours, leading to very slowing-varying error fields in an accelerator. There are also hysteresis effects[10,12].

6. Superconducting wire

The performance of the magnet is greatly dependent on the properties of the superconducting wire. The standard choice is wire fabricated from filaments of superconductor, embedded in a copper (or aluminum) matrix. The filament diameter should be small to suppress the persistent current effects noted above. The copper matrix is required for reasonable cryogenic stability. The ratio of copper to superconductor in the wire is the Cu:Sc ratio, typically around 1.5-2. The wire used for the LEP quads was rectangular in cross section, 1.8 mm x 3.6 mm, with Cu:Sc of 1.7, and containg about 2000 36 μm diameter filaments.

The quadrupole coil could be wound directly from such wire (such as usually is done for superconducting corrector magnets), or similar wires (usually called "strands" in

this case) can be bundled in parallel to form cable. Cable has higher current-carrying capacity and is favored in applications using long strings of magnets.

For the superconductor in the wire to remain in the superconducting state, the current density carried by the superconductor must be below the "critical current density" $J_{C.}$ The critical current density is a function of temperature T, field applied to the wire B, and the material properties intrinsic to the superconductor. Associated concepts are the "critical field" $B_c(T)$, which is the field at which the critical current density vanishes; and the "critical temperature" $T_c(B)$, which is the temperature at which the critical current density vanishes.

The dependence of the critical temperature on field , and vice-versa, for NbTi superconductor is[10]

$$T_c(B) = T_c(0)(1 - B / B_c(0))^{.59}$$

$$B_c(T) = B_c(0)(1 - [T / T_c(0)]^{1.7})$$

with B in Tesla and T in ^{o}K. For standard NbTi alloy, $B_c(0)$ = 14.5 T and $T_c(0)$ = 9.2 ^{o}K. In terms of these, the dependence of J_c on T and B is

$$J_c(B,T) = J_c(B_0,T_0)\left(\frac{T_c(B) - T}{T_c(B) - T_0}\right)\left(\frac{B_c(T) - B}{B_c(T) - B_0}\right)$$

This relation breaks down for B< 4T but is OK for high fields. Unlike the quantities $B_c(0)$ $T_c(0)$, which are the same for all NbTi samples, the quantity $J_C(B_0, T_0)$ is a property dependent on the metallurgy of the specific wire sample in question.

Table 6 gives examples of these quantities for the quads listed above. T_b is the bath temperature of the coils. The wire parameters have been taken all to be that of the LEP or LEP200 quads except for the RHIC case, in which the cable parameters were used. The last column gives the critical current density at the peak field in the magnet.

Table 6
Critical Temperatures, Fields and Current Densities

Quadrupole	T_0 ^{o}K	B_0 T	J_{c0} A/mm^2	T_b ^{o}K	B_{op}= Bpeak T	$T_c(B_{op})$ ^{o}K	$B_c(T_b)$ T	$J_c(B_{op},T_b)$ A/mm^2
ISR quads	4.2	5	1300	4.3	5.9	6.7	10.5	1038
LEP quads	4.2	5	1300	4.3	4.2	7.5	10.5	1452
CESR Q1	4.2	5	1300	4.6	4.9	7.2	10.	1143
CESR Q2	4.2	5	1300	4.6	5.1	7.1	10	1110
FNAL quads	4.2	5	1300	4.6	4.2	7.5	10	1328
RHIC quads	4.2	5.6	2300	4.6	3.9	7.6	10	2783
LEP 200 Quads	4.3	5	1400	4.3	5.7	6.8	10.5	1230

The critical current for a given wire (or cable) is just the critical current density times the area of superconductor. If the total wire area is A, and the copper-to-superconductor ratio is ρ, then the fraction of superconductor is

$$\varepsilon = \frac{1}{1+\rho} ,$$

and the critical current is

$$I_c(B,T) = J_c(B,T)\varepsilon A .$$

As the operating current of a magnet is increased, the peak field B increases (along the "load line"), according to

$$B = cI$$

where c is the transfer function. As B increases, the critical current decreases with B according the equations above. When the operating current exceeds the critical current, the magnet quenches. This value of I_{quench} is given by

$$J_c(cI_{quench}, T_b)\varepsilon A = I_{quench}$$

Using

$$J_c(B,T_b) = J_c(B_{op},T_b)\frac{(B_c(T_b)-B)}{(B_c(T_b)-B_{op})}$$

which is approximately correct for B near B_{op}, we get

$$I_{quench}(T_b) = \frac{B_c(T_b)}{c + \frac{B_c(T_b)-B_{op}}{J_c(B_{op},T_b)\varepsilon A}}$$

The margin at some operating current I_{op} is

$$mar(T_b) = \frac{I_{quench}(T_b)-I_{op}}{I_{op}}$$

Another measure of the margin is the temperature difference ΔT between the bath temperature and the temperature at which the margin is zero at the operating current. Using

$$J_c(B_{op},T) = J_c(B_{op},T_b)\frac{(T_c(B_{op})-T)}{(T_c(B_{op})-T_c)}$$

We get

$$\Delta T = (T_c(B_{op})-T_b)(1-\frac{I_{op}}{\varepsilon A J_c(B_{op},T_b)})$$

At $T_{bath}+\Delta T$, the current starts to flow in the copper as well as the superconductor, since the latter has gone normal. Thus $T_{bath}+\Delta T$ is called the "current-share" temperature.

Larger values of ΔT are of course preferred, since this corresponds to less sensitivity to sources of heat which can raise the local temperature enough to cause a quench.

These quantities are given in table 7 for the various quads.

Table 7
Current and temperature margins

Quadrupole	T_{bath} ^oK	B_{peak} T	I_{op} A	$I_c(B_{op},T_b)$ A/mm^2	I_{quench} A	margin %	ΔT ^oK
ISR quads	4.3	5.9	1600	2460	1887	18	0.8
LEP quads	4.3	4.1	1600	3442	2365	47.8	1.7
CESR Q1	4.6	4.9	1700	2709	2097	23	1.
CESR Q2	4.6	5.1	1700	2633	2062	21.3	0.9
FNAL quads	4.6	4.1	905	1992	1327	46	1.6
RHIC quads	4.6	3.9	5000	11831	7690	53.8	1.7
LEP 200 quads	4.3	5.7	1900	2641	2182	15	0.7

One of the consequences of the imposition of solenodial field will be a reduction in the quench current and the margin, since the operating field increases. However, except at the ends of the solenoid and the quadrupole, the longitudinal solenoidal field is normal to the radial and azimuthal quadrupole fields, so the operating field goes to

$$B_{op} \rightarrow \sqrt{B_{op}^2 + B_{sol}^2}$$

Table 8 shows the change in margin and quench current for two cases.

Table 8
Effect of solenoid field on margin

Quadrupole	B_{sol} T	B_{op} T	I_{op} A	$I_c(B_{op},T_b)$ A	I_{quench} A	margin %
LEP quads	.6	4.2	1600	3419	2360	46.9
CESR Q1	1.5	5.1	1700	2577	2037	19.8

Not much change is seen. However, near the end of the solenoid, if significant radial and/or azimuthual fields develop, the situation could change rapidly in the CESR Q1 case.

7. *Quench parameters*

Quenches in superconducting magnets are generally caused by local heating (due, for example, to frictional heat caused by conductor motion, or beam loss) which causes a local region of the superconductor to increase in temperature by more than the ΔT calculated above. The local critical current density drops below the current density in the wire, and a region of the conductor goes normal. Because of "flux-flow resistivity"[11], the

superconductor will continue to carry its critical current density, with the excess current going to the copper matrix.

Energy begins to be dissipated by Joule heating both in the copper and the normal NbTi. In the normal region, Joule heating per unit volume occurs at a rate[11]

$$G(T) = \frac{\rho\varepsilon^2 J_{op}\left[J_{op} - J_c(B_{op},T)\right]}{1-\varepsilon}$$

in which $J_{op}=I_{op}/\varepsilon A$, and ρ is the resistivity of the copper in the wire matrix. Using the expression above for the temperature dependence of the critical current density, this becomes

$$G(T) = G_c \frac{\left[T-(T_b+\Delta T)\right]}{\left[T_c(B_{op})-(T_b+\Delta T)\right]}$$

$$G_c = \frac{\rho\varepsilon^2 J_{op}^2}{1-\varepsilon}$$

For $T>T_c(B_{op})$, $G(T)$ remains constant at G_c.

Meanwhile, since the coil is still surrounded by LHe, some of the heat is conducted away. Depending on the balance between heat production and heat transport, the local region may shrink to zero (if the heat transport is sufficiently good) and the whole coil becomes superconducting again; or, if the transport is not sufficient, the normal zone will grow, generating more heat, and the whole magnet will eventually go normal: this is a quench.

If we assume that heat is transported from the wire to the LHe at a rate per unit area

$$R(T) = h(T-T_b)$$

where h= heat transfer coefficient to LHe (in watts/m^2/^{o}K), then the balance between heat transport from the wire and heat production (assuming $I_{op}=I_c$) is measured by the "Stekly parameter":

$$\alpha = \frac{G_c A}{Ph(T_c - T_b)}$$

in which P is the cooled perimeter of the wire. For $\alpha>1$, heat production exceeds cooling and the normal zone spreads and the magnet quenches; for $\alpha<1$, the normal zone shrinks and no quench occurs. In the latter case, the magnet is said to be "cryostable": it will never quench under any circumstances. This condition is rarely satisfied in superconducting magnets used for accelerators.

Using typical values for ρ (3×10^{-10} Ω–m) and h (1000 w/m^2), Table 9 gives values for G_c and α for the magnets. As can be seen, none are cryostable.

Conduction of heat longitudinally along the wire has been neglected in the previous discussion. When one considers this, one finds that, even in a magnet which is

not globally cryostable, if a sufficiently small region of the conductor goes normal, heat conduction from this region to the rest of the wire can be sufficiently large to transport all the heat generated in the small normal region away. In this case, the normal zone shrinks and no quench occurs. The length of the "minimum propagating" zone in which heat conduction just balances heat generation is given[10] by

$$l_{min} = 2\pi\sqrt{\frac{\lambda_z(T_c - T_b)}{G_c}}$$

in which λ_z is the heat conductivity along the wire(which is dominated by the heat conductivity of the copper, since that of NbTi is several orders of magntiudude smaller). λ_z has been taken to be 260 W/m/^{o}K. Normal zones smaller than l_{min}will not propagate longitudinally. Thus, local temperature rises greater than the temperture margin ΔT can occur without causing a quench, provided they do so over lengths smaller than l_{min}. Obviously, the larger l_{min}, the more stable the magnet--from this point of view, smaller values of ε (more copper in the matrix) is preferred. Table 9 gives calculated values of l_{min}.

Table 9
Cryostability parameters

Quadrupole	**J_{op} (A/mm^2)**	**P (mm)**	**G_c(mwatt /mm^3)**	α	**l_{min} (mm)**
ISR quads	675	10.8	30	7.2	29
LEP quads	675	10.8	30	5.4	33
CESR Q1	717	10.8	34	7.6	28
CESR Q2	717	10.8	34	7.8	28
FNAL quads	603	7	22	4.5	37
RHIC quads	1176	73.5	82	4.4	19
LEP 200 quads	884	8.9	51	13	23

Because the magnets will not be globally cryostable, the details of what happens when the magnet quenches need to be considered.

During a quench, the stored energy in the magnetic field ($1/2LI^2$) is dissipated: if no measures are taken to bypass the current around the magnet (i.e., there is no quench protection), this energy will all go into the magnet. The local, instantaneous energy per unit volume dissipated by Joule heating will result in a rise in the temperature of the coil:

$$\rho(T)J^2(t)dt = C(T)dT$$

Here t is time, T is temperature, and C(T) is the material's specific heat per unit volume. Integrating both sides gives

$$\int_0^\infty J^2(t)dt = \int_{T_b}^{T_{max}} \frac{C(T)dT}{\rho(T)} = F(T_{max})$$

The peak temperature which is reached by the coil, T_{max}, depends on the time integral of the square of the current density, as well as material properties of the coil. The time integral depends on how rapidly the quench develops. The quench develops by heat conduction down the wire and radially through the insulation. A rapidly developing quench spreads the energy over a large region of the coil and reduces T_{max}.. The velocity with which the quench propagates is [10]

$$v_{z,r} = \frac{J_{op}}{C}\sqrt{\frac{\rho\lambda_{z,r}}{T_c - T_b}}$$

in which $\lambda_{Z,r}$ is the longitudinal (radial) heat conductivity. Typically the radial conductivity is much smaller than the longitudinal, because of the coil insulation. Assuming simple forms for the dependence of F and ρ on temperature,

$$F(T) = F_1\sqrt{\frac{T}{T_1}} \quad \text{and} \quad \rho(T) = \rho_1\frac{T}{T_1}$$

a simple model[10,11] of the quench development leads to the following result for the time t_Q, which is characteristic of the duration of the quench:

$$t_Q = \sqrt[6]{\frac{90LF_1^2A}{4\pi J_{op}^4\rho_1 v_r^2 v_z}}$$

in which L is the inductance of the magnet. In this simple model, the quenching zone does not encounter any boundaries (like the coil edges radially, or the magnet ends longitudinally). A better approximation, which includes the effects of coil boundaries[11], reduces the quench time to

$$t'_Q = \sqrt[4]{\frac{2}{15t_a t_b}}t_Q$$

in which

$$t_a = \frac{l}{2v_z t_Q} \quad \text{and} \quad t_b = \frac{a_2 - a_1}{2v_r t_Q}$$

and l=magnet length.

Then the peak temperature in the coil is

$$T_{max} = T_1\frac{J_{op}^4 t_Q'^2}{F_1^2}$$

In table 10, the longitudinal quench velocity, quench time, and maximum temperature have been calculated for each magnet. The fixed parameters used have been T_1= 100^{o}K, ρ_1=3x10$^{-9}\Omega$-m, F_1=2.1x10^{16}A^2-sec/m^4, C= 5200 J/m^3/^{o}K, λ_z= 260 w/m/^{o}K, λ_r= .25 w/m/^{o}K.

Table 10
Quench parameters

Quadrupole	v_z (m/sec)	t'_Q(sec)	T_{max}(°K)	V_{max}(V)
ISR quads	8.5	.75	492	700
LEP quads	7.4	.62	339	803
CESR Q1	8.8	.55	346	326
CESR Q2	8.9	.62	435	375
FNAL quads	6.8	.72	255	1328
RHIC quads	13	.23	381	152
LEP 200 quads	11	.42	450	1650

It is generally accepted that peak temperatures of up to 400°K are acceptable during a quench, and pose no risk of damage to a magnet. Such a magnet thus needs no scheme to bypass the current during a quench (quench protection) and is said to be "self-protecting". The CESR quads appear to be on the edge of qualifying as self-protecting. If they can be designed to be self-protecting, this significantly simplifies the electrical system for the magnets.

Actual measurements of T_{max} in the LEP quads[2] have given $T_{max} \sim 200^o$ K.

The quench time t_Q also sets the scale for the magnitude of the eddy current forces induced in the beam tube during quench. The requirement of stability under this load usually plays a role in the choice of beam tube thickness.

During a quench, as the field collapses, the magnet inductance is effectively separated into two pieces by the normal zone.[11] Inductive voltages opposing the current change are induced across the magnet pieces, resulting in the peak voltage drop appearing across the normal zone. The size of the voltage drop is related to the rapidity of the quench, the magnet inductance and the operating current. The requirement on the (turn-to-turn) breakdown voltage of the coil insulation is set by this voltage, so it is good to minimize it. Under conservative assumptions[11], the maximum voltage drop is

$$V_{max} = \frac{2.1 L I_{op}}{t_Q} \sqrt[4]{t_a t_b}$$

Values of Vmax are shown in table 10.

Measurements in the LEP quads of the voltage across each coil have given V_{max} of 100-150 v. This is substantially less than indicated above. In the CESR quads case, voltages of no more than a few hundred volts should be expected.

8. Electrical system

The required currents for the CESR quads appear to be in the range of a 2000 A power supply. The voltage requirement on the supply is principally determined by the voltage drop in the normal bus connections, plus the inductive voltage required during current changes. For L< 0.2 H, a tuning adjustment as specified in the RFP (3% ΔI in 10 sec) requires about 1.2 volts. The bus voltages drop would be, e.g., for 200 ft. of 6 200-

MCM copper cables in parallel, about 3 volts. Thus a total voltage of 5 volts would probably be sufficient (10 kW power supply).

Although voltages during a quench do not normally appear directly across the magnet terminals, the power supply's insulation to ground should be rated for these voltages-up to 500 volts.

Current regulation requirements at low frequencies can be estimated from tune modulation considerations. The tune shift $\delta\nu$ due to a variation the focal length of a quad at β is

$$\delta\nu = \frac{\beta}{4\pi}\delta\frac{1}{f} = \frac{\beta}{4\pi f}\frac{\delta I}{I}$$

For example, for the quad Q1, $\frac{1}{f} = 1.7\ \mathrm{m}^{-1}$, $\beta_v = 65$ m so $\delta\nu = 8.8\frac{\delta I}{I}$. To limit tune modulation to $\delta\nu < 10^{-4}$, it is sufficient to have $\delta I/I \approx 10^{-5}$.

Even if no quench protection is required for the magnet, the power supply should have the ability to be turned off automatically after a quench, in a time on the order of the quench time, in order to limit additional heating of the magnet when it is in its resistive state.

9. Cryogenic system

The LEP quad cryostat refrigerator system provides, to some extent, a model for what might be done in the CESR quads case.

The LEP quad cryostat was designed for a maximum internal pressure of 4 bar. The shell was made from 304L stainless steel. No liquid nitrogen was used: the insulation of the cold mass was provided by superinsulation and a vapor-cooled heat shield. This presumably simplified the internal plumbing. The cold mass was cooled by pool-boiling LHe at 1 bar. The vapor was passed through the heat shield, used to cool the power leads (2000 A leads), and collected at room temperature. The total heat leak for the cryostat (2.5 m long) was 13 watts, including the power leads. The helium inventory in the cryostat was about 45 l. Quench relief was provided by a spring-loaded relief valve set at 3 bar; apparently, not much He was lost during a quench.

The total consumption of LHe can be estimated from

$$\dot{V}_l = \frac{\dot{Q}}{\rho L_D}$$

in which $\dot{V}_l$ is the volume of He consumed per unit time by a heat leak $\dot{Q}$, L_D is the latent heat of vaporization, and ρ the density of liquid helium. For a 20 W heat leak, this gives about 30 l/hour of LHe.

A similar system could be used for the CESR quads if the vapor could be recovered and reliquified. Also, use of pool boiling He at atmospheric pressure would

reduce the operating temperature to 4.3°K, increasing the margin in Q1 from 23% to 29%.

10. Mechanical issues-forces

The electromagnetic force per unit volume on the current density within the magnet is (neglecting end effects)

$$\vec{F}_v = \vec{J} \times \vec{B} = J_0 B_r \hat{\phi} - J_0 B_\phi \hat{r}$$

The force/length on an individual wire, of area A, carrying the current density J_0, is

$$\vec{F}_l(r,\phi) = \vec{F}_v A = J_0 A B_r(r,\phi)\hat{\phi} - J_0 A B_\phi(r,\phi)\hat{r}$$

Since B_ϕ varies like Cos(mϕ) and B_r varies like Sin(mϕ), the azimuthal component of the force is zero at ϕ=0 and maximum at $\phi=\phi_1$. Since $B_r<0$, it is in the (-ϕ) direction, and it tries to compress the coil package azimuthally, pulling it away from the coil stop at ϕ_1. The radial component of the force is in the (+r) direction at $r=a_1$, and the (-r) direction at $r=a_2$ (since B_ϕ changes sign across the radial extent of the coil). The radial force compresses the coil package radially, and is strongest at ϕ=0.

The azimuthal force pulling the coil package from the coil stop must be restrained to prevent wire motion. This is done by preloading the coil package sufficiently to ensure that it remains in compression throughout the operating range of the magnet. The precise value of the compressive preload required depends in detail on the elastic modulus of the coil package and its supports, as well as on the electromagnetic forces. However, a crude estimate of the scale of the compressive stresses can be obtained by computing the electromagnetic pressure on a wire: this is approximately

$$\underset{p}{r} \approx \frac{\vec{F}_l}{w}$$

in which $w = \frac{4A}{P}$ is a rough measure of the width dimension of the wire (A=wire area, P=wire perimeter).

Table 11 gives peak force/length and pressure for the various quads. Figures 3 and 4 show the azimuthal and radial force/length as a function of r and ϕ for the CESR Q1 case

Figure 3
Q1 coil: Azimuthal force/length

Figure 4
Q1 coil: Radial Force/length

Table 11
Electromagnetic Forces

Quadrupole	Azimuthal force/length (N/mm) $r=a_1$, $\phi=\phi_1$.	Radial force/length (N/mm) $r=a_1$, $\phi=0$	Azimuthal pressure(N/mm^2) $r=a_1$, $\phi=\phi_1$.	Radial pressure (N/mm^2) $r=a_1$, $\phi=0$
ISR quads	8.5	7.2	3.5	3.0
LEP quads	6.0	4.8	2.5	2.0
CESR Q1	7.5	6.2	3.2	2.6
CESR Q2	7.7	6.3	3.2	2.6
FNAL quads	3.3	2.9	1.4	1.2
LEP 200 quads	9.7	7.9	3.7	3.0

The actual azimuthal prestress used, for example, in the LEP200 quads[12], was about 35 N/mm^2 (350 bar).

Poor training behavior is usually due to coil motion, and this may be related to insufficient preload, although this is not always the case. Motion of the conductors in the ends, where support is more difficult, is sometimes a problem. Support of the coils in the ends is one of the more difficult mechanical problems in the fabrication of magnets. This problem will be exacerbated by the presence of an axial solenoid field. In the coil body, since such a field is parallel to the current, it exerts no force on the coils (although, as noted above, it will reduce the margin). In the ends, the current has azimuthal components, and hence there are radial forces on the coils even if the solenoid field is purely axial. Typical values of the force on one "coil package" (1/4 of the quadrupole) would be roughly

$$F_{sol} \approx B_{sol} NIa \frac{\pi}{4} = 1.5\text{Tx}200\text{x}1700\text{Ax}.08\text{mx}\frac{\pi}{4} = 3.2\text{x}10^4\text{N}$$

This force, about 7000 lb., is in the radial direction. It tries to bend the coil ends in and out (alternately).

If the solenoid fields are non-axial, then there are also forces in the body of the magnet: in addition, the margin may be further decreased. In the design of these magnets, it will be important to include the effects of the actual solenoidal field, based on the best information available, early in the design process.

11. *Conclusion*

The CESR quadrupoles can be very similar in design to existing magnets (particularly the LEP quads). The use of hundreds of turns of wire, rather than tens of turns of cable, seems preferred into order to keep the operating current in the 1500-2000 A range. Field quality requirements are stringent, but should be achievable, particularly for Q2. Persistent current multipole effects should be small at the operating point. Margins in excess of 20% should be achievable, which should mitigate training issues. The magnets will not be cryostable but may be self-protecting. The electrical system requirements are relatively modest. About 30 l/hr of He will be required; He vapor recovery would be very convenient. The use of pool-boiling He at atmospheric pressure should be considered to increase the margin. Forces on the coils are not unusually large,

but the presence of the solenoid field is a complication which needs to be included in the initial design considerations.

References

1. Spec. EN-16: Superconducting Quadrupoles for the CESR Interaction Regions: Design Study and Prototype. Technical Specifications (May 31, 1995)

2. Ph. Lebrun et al, "Design, Test and Performance of the Prototype Superconducting Quadrupole for the LEP Low-beta insertions", IEEE Trans. on Magnetics, 24, 2 (1361-4), 1988

3. P. J. Ferry et al, "analysis of the Performance of the Eight Superconducting Quadrupoles for the LEP Low-beta insertion", CERN LEP-MA/89-67 (1989)

4. K. Tsuchiya et al, "Superconducting Quadrupole Magnets for the TRISTAN Low-beta insertion", KEK Preprint 89-65 (1989)

5. K. Tsuchiya et al, "A prototype Superconducting insertion quadrupole magnet for TRISTAN", Advances in Cryogenic Engineering, Vol. 31 (173) 1986

6. K. Tsuchiya et al, "Cryogenic System of the Superconducting insertion quadrupole magnet for the TRISTAN Main Ring", Advances in Cryogenic Engineering, 35B (941) 1990

7. R. Gupta et al, "Large Aperture Quadrupoles for the RHIC Interaction regions, Proc. of the 1993 Particle Accelerator Conference (2745) 1993

8. R.P.Smith et al, "Performance results of a Low Current, High Gradient Superconducting Quadrupole Magnet", IEEE Trans. on Nucl. Sci., NS-30,4(3672) 1983

9. J. Billan et al, "The eight superconducting quadrupoles for the ISR high-luminosity insertion" Proc. of the XIth International Conference on High-Energy Accelerators, 1980 (848-852)

10. K. H. Meβ, P. Schmuser, "Superconducting Accelerator Magnets", in "Proceedings of CAS-Superconductivity in Particle Accelerators", pg. 87 (1989)

11. M. N. Wilson, "Superconducting Magnets", Oxford (1983)

12. A. Ijspeert, T. M. Taylor, M. Begg, "Construction and Test of Superconducting Quadrupoles for the LEP2 Low-Beta Insertion".

Appendices

Appendix 1: Vector potential for a single-shell quadrupole

We wish to evalute the integral

$$A_z(r,\phi) = \int_0^\infty ada \int_0^{2\pi} d\phi' J(a,\phi') \frac{dA_z(r,\phi,a,\phi')}{dI}$$

in which J and dA_z/dI are given above in the text. The result will have the general form

$$A_z^{coil}(r,\phi) = \frac{\mu_0 J_0}{2\pi}\sum_{n=1}^{\infty}\frac{1}{n}R_n(r,a_1,a_2)\Phi_n(\phi,\phi_1)$$

in which

$$\begin{aligned}\Phi_n(\phi,\phi_1) &= \int_{-\phi_1}^{\phi_1} d\phi' \mathrm{Cos}[n(\phi-\phi')] + \int_{\pi-\phi_1}^{\pi+\phi_1} d\phi' \mathrm{Cos}[n(\phi-\phi')] \\ &\quad - \int_{\frac{\pi}{2}-\phi_1}^{\frac{\pi}{2}+\phi_1} d\phi' \mathrm{Cos}[n(\phi-\phi')] - \int_{\frac{3\pi}{2}-\phi_1}^{\frac{3\pi}{2}+\phi_1} d\phi' \mathrm{Cos}[n(\phi-\phi')] \\ &= \mathrm{Re}\int_{-\phi_1}^{\phi_1} d\phi' \begin{bmatrix} \mathrm{Exp}\{in(\phi-\phi')\} + \mathrm{Exp}\{in(\phi-\phi'-\pi)\} \\ -\mathrm{Exp}\{in(\phi-\phi'-\frac{\pi}{2})\} - \mathrm{Exp}\{in(\phi-\phi'-\frac{3\pi}{2})\} \end{bmatrix}\end{aligned}$$

and

$$\begin{aligned}R_n(r,a_1,a_2) &= \int_{a_1}^{a_2} ada \begin{Bmatrix} \left(\frac{r}{a}\right)^n & \text{for } r < a_1 \\ \left(\frac{a}{r}\right)^n & \text{for } r > a_2 \end{Bmatrix} \\ &= \int_{a_1}^{r} ada\left(\frac{r}{a}\right)^n + \int_{r}^{a_2} ada\left(\frac{a}{r}\right)^n \quad \text{for } a_1 < r < a_2\end{aligned}$$

The angular integral is

$$\Phi_n(\phi,\phi_1) = \mathrm{Re}\begin{bmatrix} (1+\mathrm{Exp}\{-in\pi\} - \mathrm{Exp}\{-in\frac{\pi}{2}\} - \mathrm{Exp}\{-in\frac{3\pi}{2}\}) \\ \mathrm{Exp}\{in\phi\}\int_{-\phi_1}^{\phi_1} d\phi' \mathrm{Exp}\{-in\phi'\} \end{bmatrix}$$

$$\begin{aligned}\Phi_n(\phi,\phi_1) &= \frac{2}{n}\mathrm{Sin}\ \ n\phi_1\, \mathrm{Re}\left[\mathrm{Exp}\{in\phi\}(1+(-1)^n)(1-i^n)\right] \\ &= \begin{Bmatrix} \frac{8}{n}\mathrm{Sin}\ \ n\phi_1 \mathrm{Cos}\ \ n\phi\ ,\ n = 2,6,10,\ldots \\ 0\ \ \text{otherwise} \end{Bmatrix}\end{aligned}$$

Equivalently, using n=2m,

$$\Phi_m(\phi,\phi_1) = \frac{4}{m}\mathrm{Sin}\ \ 2m\phi_1 \mathrm{Cos}\ \ 2m\phi,\ \ m\ \ \text{odd}$$

The radial integral is

$$\text{For } r < a_1 \quad R_m(r,a_1,a_2) = \frac{r^2}{2-2m}\left(\left[\frac{r}{a_2}\right]^{2m-2} - \left[\frac{r}{a_1}\right]^{2m-2}\right)$$

$$\text{For } r > a_2 \quad R_m(r,a_1,a_2) = \frac{r^2}{2m+2}\left(\left[\frac{a_2}{r}\right]^{2m+2} - \left[\frac{a_1}{r}\right]^{2m+2}\right)$$

For $a_1 < r < a_2$

$$R_m(r,a_1,a_2) = r^2\left(\frac{1}{2m+2} - \frac{1}{2-2m}\right) + \frac{r^2}{2-2m}\left[\frac{r}{a_2}\right]^{2m-2} - \frac{r^2}{2m+2}\left[\frac{a_1}{r}\right]^{2m+2}$$

These equations are not valid for $r<a_2$ and m=1: in this case, the results are

$$\text{For } a_1 < r < a_2 \quad R_m(r,a_1,a_2) = \frac{1}{4}\left(r^2 - \frac{a_1^4}{r^2}\right) + r^2 \ln\frac{a_2}{r}$$

$$\text{For } r < a_1 \quad R_m(r,a_1,a_2) = r^2 \ln\frac{a_2}{a_1}$$

In terms of these integrals, then,

$$A_z^{coil}(r,\phi) = \frac{\mu_0 J_0}{2\pi} \sum_{m \text{ odd}} \frac{1}{2m} R_m(r,a_1,a_2)\Phi_m(\phi,\phi_1)$$

Appendix 2: Effects due to iron shell at $r=R_e$

The effect of an iron shell at $r=R_e$, centered at r=0, can be included as follows, for the case of iron with a homogeneous, isotropic permeability μ.

Let there be a line current I at (a,ϕ'), located in a cylindrical cavity of inner radius R_e, centered at r=0, in an infinite iron block of permeability μ. Then the field inside the cavity due to the iron is equivalent to that produced by an image line current of magnitude I' located at (a',ϕ'), where

$$a' = \frac{R_e^2}{a} \text{ and } I' = \frac{\mu-\mu_0}{\mu+\mu_0} I.$$

For a quadrupole current distribution as described above within the cavity, the effect of the iron inside the cavity is equivalent to a (non uniform) image current density

$$J_0'(a') = \frac{\mu-\mu_0}{\mu+\mu_0} J_0 \frac{R_e^4}{a'^4}$$

extending from $a_2' = \frac{R_e^2}{a_2}$ to $a_1' = \frac{R_e^2}{a_1}$. This current density results in an additional contribution to the vector potential,

$$A_z^{iron}(r,\phi) = \frac{\mu_0 J_0}{2\pi}\frac{\mu-\mu_0}{\mu+\mu_0}\sum_{m\ odd}\frac{1}{2m}R_m^{iron}(r,a_1,a_2)\Phi_m(\phi,\phi_1)$$

in which

$$R_m^{iron}(r,a_1,a_2) = \frac{r^2\left(r/R_e\right)^{4m}}{2m+2}\left[\left(\frac{a_2}{r}\right)^{2m+2} - \left(\frac{a_1}{r}\right)^{2m+2}\right]$$

The total vector potential for points inside the cavity in the iron is then

$$A_z^{tot}(r,\phi) = A_z^{coil}(r,\phi) + A_z^{iron}(r,\phi)$$

For a single line current I within the cavity at (a,ϕ'), the vector potential in the region in the iron, $r>R_e$, is that due to a line current I'' in the cavity at (a,ϕ'), where

$$I'' = I\frac{2\frac{\mu}{\mu_0}}{\mu+\mu_0}$$

There is also an image line current at r=0, but when one considers the image current distribution of a quadrupole current shell, which has net total current zero, the total image current at r=0 sums to zero. Thus for $r>R_e$, the vector potential is just

$$A_z^{tot}(r,\phi) = \frac{2\frac{\mu}{\mu_0}}{\mu+\mu_0}A_z^{coil}(r,\phi)$$

Appendix 3: Inductance/length

The inductance per unit length of the magnet (L_l) can be calculated from these equations using the expression for the energy stored in the magnetic field,

$$W_l = \frac{1}{2}\int_0^\infty r dr \int_0^{2\pi} d\phi \vec{J}\bullet\vec{A} = \frac{1}{2}L_l I^2$$

with

$$A_z(r,\phi) = \frac{\mu_0 J_0}{2\pi}\sum_{m\ odd}\frac{1}{2m}\left(R_m^{coil}(r,a_1,a_2) + \frac{\mu-\mu_0}{\mu+\mu_0}R_m^{iron}(r,a_1,a_2)\right)\Phi_m(\phi,\phi_1)$$

and J as given above in the text, we have

$$W_l = \frac{\mu_0 J_0^2}{4\pi} \int_{a_1}^{a_2} \sum_{m\ odd} \frac{1}{2m} (R_m^{coil}(r,a_1,a_2) + \frac{\mu-\mu_0}{\mu+\mu_0} R_m^{iron}(r,a_1,a_2)) r dr$$

$$\text{Re} \int_{-\phi_1}^{\phi_1} d\phi \text{Exp}(2im\phi)\left[1 + \text{Exp}(-2\pi i m) - \text{Exp}(-\pi i m) - \text{Exp}(-3\pi i m)\right]$$

$$\frac{4}{m} \text{Sin}[2m\phi_1]$$

The angular integral is

$$\frac{\text{Sin}[2m\phi_1]}{m}(1-(-1)^m) = \frac{2\text{Sin}[2m\phi_1]}{m} \text{ for m odd}$$

The radial integral is

$$I_m^{coil} = \int_{a_1}^{a_2} R_m^{coil}(r,a_1,a_2) r dr = \frac{a_2^4(2m-2-(2m+2)r^4+4r^{2m+2})}{2(2m-2)(2m+2)} \text{ for } m \neq 1$$

$$= \frac{a_2^4(1+r^4(4\text{Log}(r)-1))}{8} \text{ for } m = 1$$

$$I_m^{iron} = \int_{a_1}^{a_2} R_m^{iron}(r,a_1,a_2) r dr = \frac{a_2^4(r^{2m+2}-1)^2}{(2m+2)^2} \left(\frac{a_2}{R_e}\right)^{4m}$$

in which $r = \frac{a_1}{a_2}$.

Then

$$W_l = \frac{2\mu_0 J_0^2}{\pi} \sum_{m\ odd} \frac{\text{Sin}^2[2m\phi_1]}{m^3} (I_m^{coil}(r,a_1,a_2) + \frac{\mu-\mu_0}{\mu+\mu_0} I_m^{iron}(r,a_1,a_2))$$

Using $J_0 = \frac{2NI}{\phi_1(a_2^2-a_1^2)}$ we get

$$W_l = \frac{8\mu_0 N^2 I^2}{\pi\phi_1^2(a_2^2-a_1^2)^2} \sum_{m\ odd} \frac{\text{Sin}^2[2m\phi_1]}{m^3} (I_m^{coil}(r,a_1,a_2) + \frac{\mu-\mu_0}{\mu+\mu_0} I_m^{iron}(r,a_1,a_2))$$

so

$$L_l = \frac{16\mu_0 N^2}{\pi\phi_1^2(a_2^2-a_1^2)^2} \sum_{m\ odd} \frac{\text{Sin}^2[2m\phi_1]}{m^3} (I_m^{coil}(r,a_1,a_2) + \frac{\mu-\mu_0}{\mu+\mu_0} I_m^{iron}(r,a_1,a_2))$$

Appendix 4: Field harmonics

Using

$$B_\phi(r,\phi) = -\frac{\mu_0 J_0}{4\pi} \sum_{m\ odd} \frac{1}{m} \frac{dR_m(r,a_1,a_2)}{dr} \Phi_m(\phi,\phi_1)$$

and

$$\Phi_m(\phi,\phi_1) = \frac{4}{m} \text{Sin}\ 2m\phi_1 \text{Cos}\ 2m\phi,$$

and

$$R_m(r,a_1,a_2) = r^{2m} \left\{ \frac{\left(a_2{}^{2-2m} - a_1{}^{2-2m}\right)}{2-2m} + \frac{\mu-\mu_0}{\mu+\mu_0} \frac{\left[a_2{}^{2m+2} - a_1{}^{2m+2}\right]\left(1/R_e\right)^{4m}}{2m+2} \right\}$$

$$= r^{2m} s(m)$$

We get

$$B_\phi(r,\phi) = -\frac{2\mu_0 J_0}{\pi} \sum_{m\ odd} \frac{r^{2m-1} s(m)}{m} \text{Sin}\ 2m\phi_1 \text{Cos}\ 2m\phi$$

The reference field is

$$B_0 = -\frac{2\mu_0 J_0}{\pi} r_0 s(1) \text{Sin}\ 2\phi_1$$

so

$$B_\phi(r,\phi) = \frac{B_0}{r_0 s(1) \text{Sin}\ 2\phi_1} \sum_{m\ odd} \frac{r^{2m-1} s(m)}{m} \text{Sin}\ 2m\phi_1 \text{Cos}\ 2m\phi$$

Equating like coefficients of the harmonic functions, we conclude that b_n=0 for n even, and a_n=0 for all n; otherwise, b_{2m}=0 for m even, and for m odd,

$$\left[\frac{r}{r_0}\right]^{2m-1} B_0 b_{2m} = \frac{B_0}{r_0 s(1) \text{Sin}\ 2\phi_1} \frac{r^{2m-1} s(m)}{m} \text{Sin}\ 2m\phi_1,$$

$$b_{2m} = r_0^{2m-2} \frac{s(m)}{m s(1)} \frac{\text{Sin}\ 2m\phi_1}{\text{Sin}\ 2\phi_1}$$

in which

$$\frac{s(m)}{m s(1)} = \frac{\left\{ \frac{\left(a_2{}^{2-2m} - a_1{}^{2-2m}\right)}{2-2m} + \frac{\mu-\mu_0}{\mu+\mu_0} \frac{\left[a_2{}^{2m+2} - a_1{}^{2m+2}\right]\left(1/R_e\right)^{4m}}{2m+2} \right\}}{m\left\{ \ln\frac{a_2}{a_1} + \frac{\mu-\mu_0}{\mu+\mu_0} \frac{\left[a_2{}^4 - a_1{}^4\right]}{4R_e^4} \right\}}$$

Using $a_2 = a_1(1+\frac{\Delta a}{a_1})$, and keeping terms of first order in $\Delta a/a_1$ only, gives

$$\frac{s(m)}{ms(1)} \approx \frac{\left\{ a_1^{\,2-2m} + \frac{\mu-\mu_0}{\mu+\mu_0}\frac{a_1^{\,2m+2}}{R_e^{4m}} \right\}}{m\left\{1+\frac{\mu-\mu_0}{\mu+\mu_0}\frac{a_1^{\,4}}{R_e^4}\right\}}$$

and so

$$b_{2m} = \frac{\left\{ \left[\frac{r_0}{a_1}\right]^{2m-2} + \frac{\mu-\mu_0}{\mu+\mu_0}\left(\frac{a_1 r_0}{R_e^2}\right)^{2m}\left(\frac{a_1}{r_0}\right)^2 \right\}}{m\left\{1+\frac{\mu-\mu_0}{\mu+\mu_0}\frac{a_1^{\,4}}{R_e^4}\right\}} \frac{\text{Sin } 2m\phi_1}{\text{Sin } 2\phi_1}$$